PERGAMON

Journal of Atmospheric and Solar-Terrestrial Physics 65 (2003) 1151–1160

Journal of ATMOSPHERIC AND SOLAR-TERRESTRIAL PHYSICS

www.elsevier.com/locate/jastp

Method of auxiliary sources for calculating the magnetic and electric fields induced in a layered Earth

Simon G. Shepherd*, Fridon Shubitidze

Thayer School of Engineering, Dartmouth College, 8000 Cummings Hall, Hannover, NH 03755-8000, USA

Received 18 November 2002; received in revised form 4 June 2003; accepted 18 June 2003

Abstract

Time varying ionospheric currents caused by geomagnetic storms originating from the Sun induce electric currents in expansive technological networks located on the Earth's surface. These so-called geomagnetically induced currents (GICs) can be damaging to the systems in which they flow. The ability to estimate the magnitude of GICs is, therefore, desirable in order to mitigate any serious effects from this common space weather occurrence. A necessary element in determining GICs is the accurate calculation of the geoelectric field due to ionospheric current sources. Until now, methods for calculating these fields have primarily focused on computational efficiency. These methods are inaccurate to varying degrees and almost entirely restricted to layered or one-dimensional models of the Earth's conductivity. This work introduces a new technique to the geomagnetic induction problem known as the method of auxiliary sources (MAS). The MAS uses elementary electric/magnetic currents placed on auxiliary surfaces to produce the fields resulting from the primary ionospheric current and secondary currents induced in the Earth. Numerical results for a single- and two-layer Earth model show that the MAS is extremely accurate over the frequency range of interest in geomagnetic induction (0–1 Hz). The MAS is not, however, limited to layered Earth models and can be used with general three-dimensional structures. Furthermore, it is shown that by using the MAS, it is possible to determine the fields at any location and with any resolution on the surface or within the Earth. The combination of accuracy and flexibility demonstrate the potential of the MAS for studying complicated geomagnetic induction problems.

Keywords: Geoelectric field; Ionospheric currents; Method of auxiliary sources; Geomagnetically induced currents; Geomagnetic induction

1. Introduction

Geomagnetic storms originating from the Sun can cause large, rapidly varying currents to flow in the Earth's ionosphere which in turn can induce significant electrical currents in nearby technological networks, such as power transmission grids, telecommunication cables, pipelines, and railways. The process by which these so-called geomagnetically induced currents (GICs) are produced is further complicated by contributions from secondary currents which flow within the Earth and are frequency dependent. The effects of GICs can be damaging, even catastrophic, to the systems in which they flow (Boteler et al., 1998, and references therein). As these networks become increasingly interconnected and expansive, the potential for large GICs and damage to these systems also increases (Molinski et al., 2000).

The determination of GICs in any technological system is typically divided into two parts: (1) the geomagnetic induction process and (2) the engineering portion. The latter part is a rather straightforward task which essentially involves integration of the induced horizontal electric field (geoelectric field) over the path of the conductor of interest, taking care to include boundary conditions such as ground points along the way. This step is specific to each system and relatively simple matrix methods are well-known for calculating the GIC given the induced geoelectric field at the surface of the Earth and the geometry of the system (e.g., Lehtinen and Pirjola, 1985).

* Corresponding author. Tel.: 1-603-646-0096; fax: 1-603-646-3856.

E-mail address: simon@thayer.dartmouth.edu (S.G. Shepherd).

1364-6826/$ - see front matter © 2003 Elsevier Ltd. All rights reserved.
doi:10.1016/S1364-6826(03)00159-7

The accuracy of the resulting GIC, however, strongly depends on the determination of the induced geoelectric field and is the topic of this paper. This step, in general, is a rather complicated process involving electromagnetic induction in a non-homogeneous conducting medium from a spatially distributed, time varying current source. Understanding the relative importance of these processes is critical to a better understanding of GICs and ultimately to mitigating their effects.

Much of the recent work in calculating geoelectric fields has focused on a technique known as the complex image method (CIM), whereby the inductive properties of the Earth are incorporated by the use of 'image' currents located at complex depths (see Section 2.3 for further details). The geoelectric and geomagnetic fields calculated at the surface of the Earth using the CIM have been shown to agree very well with exact calculations for several models of the Earth's conductivity structure (Boteler and Pirjola, 1998; Pirjola and Viljanen, 1998; Pirjola and Boteler, 2002). The algebraic expressions for these fields lead to very rapid computation making the CIM a desirable method for investigating geomagnetic induction and the resulting GICs (Viljanen et al., 1999a, b; Boteler and van Beek, 1999; Boteler et al., 2000; Pulkkinen et al., 2000; Pirjola et al., 2000; Pirjola, 2000).

The CIM is, however, limited in its accuracy and ultimately restricted to one-dimensional (1D) layered Earth models. A more accurate and sophisticated technique is necessary to investigate geomagnetic induction for realistic situations that include horizontal variations in conductivity, such as coastal regions near land/sea interfaces. The method of auxiliary sources (MAS) is shown in this work to be exact for 1D layered Earth models, but is in no way limited to 1D models, and, therefore, may be an ideal technique for more complicated geomagnetic induction problems.

The MAS is a numerical technique which was originally developed for solving a wide class of scattering and radiation electromagnetic problems (Shubitidze et al., 2002a, b; Anastassiu et al., 2002, and references therein). Recently, the MAS has been applied to various low-frequency electromagnetic induction problems (Shubitidze et al., 2002c, d). It has been widely demonstrated to be a general, robust, and accurate numerical method for low-frequency electromagnetic induction scattering by highly conducting and permeable targets. Particularly in application to composite objects, the reduced computational complexity of the method shows great potential for simulating realistically complex electromagnetic induction problems (Shubitidze et al., 2001).

Briefly, in the MAS, boundary value problems are solved numerically by representing the electromagnetic fields in each domain of the structure under investigation by a finite linear combination of analytic solutions of the relevant field equations, corresponding to sources situated at some distance away from the boundaries of each domain. The 'auxiliary sources' producing these analytical solutions are chosen to be elementary currents and charges located on fictitious auxiliary surface(s), usually conforming to the actual surface(s) of the structure. In practice, at least as the method is realized here, we only require points on the auxiliary and actual surfaces, without resorting to the detailed mesh structures as required by other methods (finite element method, boundary element method, etc.). The two auxiliary surfaces are set up inside and outside the penetrable scattering object. Specifically, the fields outside of the structure are considered to originate from a set of auxiliary sources placed inside the object, and the fields penetrating inside the object arise from a set of auxiliary sources placed outside the object. The fields constructed inside and outside of the object are required to obey the continuity and jump condition of the tangential and normal magnetic field ($\mathbf{H}$) components, respectively, at an array of selected points on the surface(s) of the structure. The result is a set of matrix equations in which the amplitudes of auxiliary sources are to be determined. Once the amplitude of auxiliary sources is found the solution is complete; the magnetic and electric fields and related parameters can easily be computed throughout the interior and exterior domains.

This work describes the use of a two-dimensional (2D) frequency-domain MAS code to calculate the electric and magnetic fields in a 1D layered Earth produced by a line current source. The rest of the paper is organized as follows: Section 2.1 describes the MAS technique and Sections 2.2 and 2.3 describe the integral solution to Maxwell's equations and the CIM. In Section 3 the resulting fields from the various methods are compared for a single- (Section 3.1) and two-layer (Section 3.2) Earth. Finally, in Section 3.3 the fields inside the two-layer Earth model are discussed.

2. Techniques

This section describes the various techniques used to calculate the geoelectric and geomagnetic fields at the surface of the Earth. A 1D layered-Earth conductivity model is used in order that comparisons to other methods can be made. Fig. 1 shows the general configuration for two different Earth models, a single- and a two-layer model, where the bottom layer is a semi-infinite half-space in both cases. A constant electric line current I is located at a height h above the Earth surface, is directed in the $+\hat{\mathbf{y}}$ direction, and extends to infinity in both $\pm\hat{\mathbf{y}}$ directions. The fields, therefore, have no y-dependence (2D).

2.1. Method of auxiliary sources (MAS)

To describe the application of the MAS to the geomagnetic induction situation, a single-layer Earth conductivity model is used as an example (see Fig. 2). For future convenience, the semi-infinite half-spaces defined by $z < 0$ and $z > 0$ are referred to as regions 1 and 2, respectively. The primary magnetic field from the ionospheric current pene-

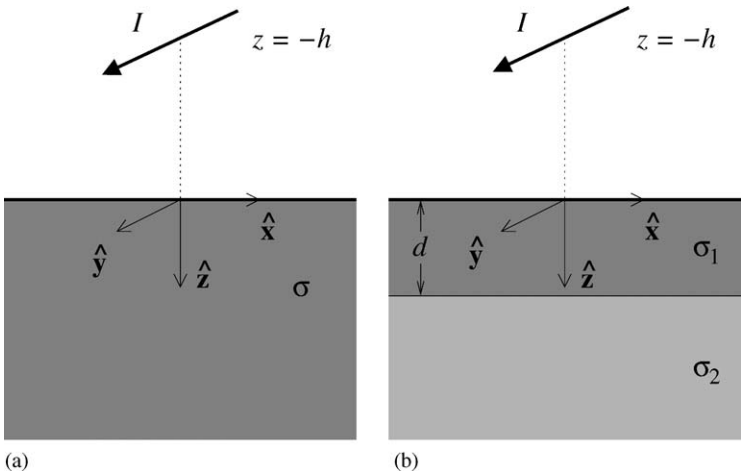

Fig. 1. (a) A single semi-infinite half-space Earth model with conductivity σ and (b) a two-layer model with a top layer thickness of d and conductivities σ_1 and σ_2. A line current, I, is located above the Earth's surface at height h.

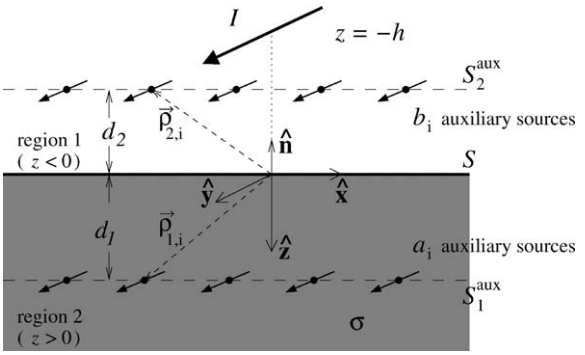

Fig. 2. MAS geometry for a 1D single-layer Earth conductivity model.

trates the Earth and produces eddy currents in the ground. The result is a secondary or scattered field in region 1. It is well established that in the frequency regime considered here (0–1 Hz) the displacement currents ($\partial D/\partial t$) are negligible in both regions 1 and 2 (e.g., Kaufman and Keller, 1981). Considering the vector potential $\mathbf{A}$ in Maxwell's equations, the following differential equations hold:

$$\nabla^2 \mathbf{A}_1 = 0, \quad \text{region 1}, \tag{1}$$

$$\nabla^2 \mathbf{A}_2 - \mathrm{j}\omega\mu\sigma \mathbf{A}_2 = 0, \quad \text{region 2}, \tag{2}$$

where $\mathrm{j} = \sqrt{-1}$, $\mu = \mu_0\mu_r$ is the magnetic permeability of the Earth, and μ_r is the relative magnetic permeability. Here a time dependence of $e^{j\omega t}$ is assumed and is subsequently suppressed throughout the paper. The Earth is considered to be non-permeable ($\mu_r = 1$) with uniform conductivity σ and the conductivity of air (region 1) is assumed to be 0.

The magnetic and electric fields in regions 1 and 2 can be expressed as

$$\mathbf{H}_\alpha = \nabla \times \mathbf{A}_\alpha, \tag{3}$$

$$\mathbf{E}_\alpha = -\mathrm{j}\omega \mathbf{A}_\alpha, \tag{4}$$

where $\alpha = 1$ or 2, respectively. The magnetic fields in regions 1 and 2 are linked by the following boundary conditions at $z = 0$:

$$\hat{\mathbf{n}} \times (\mathbf{H}_1^{sc} + \mathbf{H}^{pr}) = \hat{\mathbf{n}} \times \mathbf{H}_2, \tag{5}$$

$$\hat{\mathbf{n}} \cdot (\mathbf{H}_1^{sc} + \mathbf{H}^{pr}) = \hat{\mathbf{n}} \cdot \mathbf{H}_2, \tag{6}$$

where $\hat{\mathbf{n}}$ is a unit normal vector on the real surface S, i.e., the surface of the Earth. The magnetic field outside of the Earth (region 1: $z < 0$) is the sum of two components, the primary field ($\mathbf{H}^{pr}$) due to the line current and the scattered field in region 1 ($\mathbf{H}_1^{sc}$) due to induced eddy currents distributed within the conducting Earth. $\mathbf{H}_2$ is the total magnetic field inside the Earth (region 2: $z > 0$).

According to the MAS for penetrable objects, two auxiliary surfaces, S_1^{aux} and S_2^{aux}, are required to describe the fields in both regions 1 and 2, respectively (Shubitidze et al., 2002b). Fig. 2 shows the location of these surfaces.

The secondary magnetic field in region 1 ($\mathbf{H}_1^{sc}$) due to the induced Earth currents, is represented as a superposition of the magnetic field generated from the finite number (N) of line currents located on surface S_1^{aux}. These line currents have amplitudes $\{a_i\}$, where $i = 1, 2, 3, \ldots, N$, are located at positions $\{\boldsymbol{\rho}_{1,i}\} = \{x_{1,i}\hat{\mathbf{x}} + z_{1,i}\hat{\mathbf{z}}\}$, and are directed in the $+\hat{\mathbf{y}}$ direction. It is noted that the auxiliary surface S_1^{aux} is enclosed by the physical surface S. The auxiliary currents

$\{a_i\}$ radiate as if in an unbounded free space with region 1 characteristics and, therefore, give rise to the secondary field,

$$\mathbf{H}_1^{\mathrm{sc}}(\boldsymbol{\rho}) = \sum_{i=1}^{N} \mathbf{H}_{1,i}^{\mathrm{sc}}(\boldsymbol{\rho}, \boldsymbol{\rho}_{1,i}) = \sum_{i=1}^{N} \nabla \times \mathbf{A}_{1,i}^{\mathrm{sc}}(\boldsymbol{\rho}, \boldsymbol{\rho}_{1,i}), \tag{7}$$

where $\boldsymbol{\rho} = x\hat{\mathbf{x}} + z\hat{\mathbf{z}}$, $\mathbf{H}_{1,i}^{\mathrm{sc}}(\boldsymbol{\rho}, \boldsymbol{\rho}_{1,i})$ is the secondary field resulting from the single auxiliary current source a_i, and $\mathbf{A}_{1,i}^{\mathrm{sc}}(\boldsymbol{\rho}, \boldsymbol{\rho}_{1,i})$ is the fundamental solution of the governing Eq. (1) in region 1

$$\mathbf{A}_{1,i}^{\mathrm{sc}}(\boldsymbol{\rho}, \boldsymbol{\rho}_{1,i}) = \frac{a_i}{4\pi} \ln|\boldsymbol{\rho} - \boldsymbol{\rho}_{1,i}|\hat{\mathbf{y}}. \tag{8}$$

The total magnetic field in region 1 is, therefore, simply $\mathbf{H}^{\mathrm{pr}} + \mathbf{H}_1^{\mathrm{sc}}$, where

$$\mathbf{A}_1^{\mathrm{pr}}(\boldsymbol{\rho}) = \frac{I}{4\pi} \ln\sqrt{x^2 + (z+h)^2}\hat{\mathbf{y}}, \tag{9}$$

the vector potential due to the line current source located at position $(x = 0, z = -h)$, and with amplitude I.

Similarly, the induced fields in region 2 are constructed from the superposition of the fields generated by a finite number (N) of line current sources located on surface S_2^{aux}, with amplitudes $\{b_i\}$, located at positions $\{\boldsymbol{\rho}_{2,i}\} = \{x_{2,i}\hat{\mathbf{x}} + z_{2,i}\hat{\mathbf{z}}\}$, and directed in the $+\hat{\mathbf{y}}$ direction. The surface S_2^{aux} also encloses the interface S and the current sources $\{b_i\}$ radiate in an unbounded homogeneous space filled with the Earth's material properties (σ) producing the internal induced magnetic field,

$$\mathbf{H}_2(\boldsymbol{\rho}) = \sum_{i=1}^{N} \mathbf{H}_{2,i}(\boldsymbol{\rho}, \boldsymbol{\rho}_{2,i}) = \sum_{i=1}^{N} \nabla \times \mathbf{A}_{2,i}(\boldsymbol{\rho}, \boldsymbol{\rho}_{2,i}), \tag{10}$$

where $\mathbf{H}_{2,i}(\boldsymbol{\rho}, \boldsymbol{\rho}_{2,i})$ is the field resulting from the single auxiliary current source b_i, and $\mathbf{A}_{2,i}(\boldsymbol{\rho}, \boldsymbol{\rho}_{2,i})$ is the fundamental solution of the governing Eq. (2) in region 2

$$\mathbf{A}_{2,i}(\boldsymbol{\rho}, \boldsymbol{\rho}_{2,i}) = \frac{b_i}{4\pi} K_0(k|\boldsymbol{\rho} - \boldsymbol{\rho}_{2,i}|)\hat{\mathbf{y}}, \tag{11}$$

$K_0()$ being the modified zero order Bessel function and $k = \sqrt{-\mathrm{j}\omega\sigma\mu}$ is the induction number in region 2.

Enforcing the boundary conditions, Eqs. (5) and (6), at N points on the physical boundary S, a sufficient number of independent linear equations can be generated to determine the unknown sets of coefficients $\{a_i\}$ and $\{b_i\}$. The vector potentials are, therefore, determined outside $(z \leqslant 0)$ and inside $(z \geqslant 0)$ the Earth by Eqs. (8)–(9) and Eq. (11), respectively. The total magnetic and electric fields in each region are then given by Eqs. (3) and (4).

It has been shown that the distances between the physical surface S and auxiliary surfaces S_1^{aux} and S_2^{aux} have a significant affect on the accuracy and convergence rate of the solution of Eqs. (5) and (6) (Shubitidze et al., 2002a, b; Anastassiu et al., 2002, and references therein). For high-frequency scattering and excitation problems these distances must enclose the scattered field singularities possessed by analytical continuation of the scattered field inside the object (Shubitidze et al., 2002a; Anastassiu et al., 2002, and references therein). However, these rules did not apply in the low-frequency electromagnetic induction problem. The distances are, therefore, determined intuitively based on satisfaction of the boundary conditions and experience. For reference, the calculations for the single-layer Earth conductivity model (Fig. 2) were performed with $d_1 = d_2 = 50$ km, $N = 700$, and a separation of 25 km between auxiliary sources.

To extend the MAS to the two-layer Earth model shown in Fig. 1b, two additional auxiliary surfaces S_3^{aux} and S_4^{aux} and appropriate sets of line current sources are added on either side of the physical boundary between the two Earth layers. Additional boundary conditions at the interface at depth d provide the necessary equations to determine all the unknown sets of coefficients and, therefore, the vector potentials $\mathbf{A}_\alpha$, where now $\alpha = 1, 2$, or 3 for the three separate regions. The solutions to the fields both inside and outside the Earth are obtained by the appropriate field Eqs. (3) and (4).

2.2. Maxwell's integral equations

For comparison, Maxwell's equations, neglecting the displacement current, may be used to derive integral equations for the electric and magnetic fields in the Earth due to an ionospheric current source. Hermance and Peltier (1970) derive the following 2D field equations, valid at the surface of the Earth, resulting from a horizontal line current located at a height $z = -h$:

$$B_x = \frac{\mu_0 I}{2\pi} \int_0^\infty (1+R)\mathrm{e}^{-hv} \cos vx \, \mathrm{d}v, \tag{12}$$

$$B_z = -\frac{\mu_0 I}{2\pi} \int_0^\infty (1-R)\mathrm{e}^{-hv} \sin vx \, \mathrm{d}v, \tag{13}$$

$$E_y = -\frac{\mathrm{j}\omega\mu_0 I}{2\pi} \int_0^\infty \frac{1}{v}(1-R)\mathrm{e}^{-hv} \cos vx \, \mathrm{d}v, \tag{14}$$

where I is the amplitude of the current, ω is the frequency, and x is the horizontal distance from the current along the Earth's surface. The integration variable v results from the Fourier decomposition of the line current into horizontal structure.

The reflection coefficient, R, is in general, a complex function of the Earth's conductivity structure. Here only the relations for the single- and two-layer Earth conductivity models shown in Fig. 1 are given. The extension to an N-layered model is quite straightforward using a recursion relation such as that given by Kaufman and Keller (1981, p. 70).

Using slightly different notation, Hermance and Peltier (1970) give the following expression for the reflection coefficient of a 1D, two-layer Earth model:

$$R^{2\mathrm{L}} = \frac{(\theta_1 - v) + (\theta_1 + v)K\mathrm{e}^{-2\theta_1 d}}{(\theta_1 + v) + (\theta_1 - v)K\mathrm{e}^{-2\theta_1 d}}, \tag{15}$$

where

$$K = \frac{\theta_2 - \theta_1}{\theta_2 + \theta_1}, \tag{16}$$

the thickness of the top layer is d, and the conductivities of the upper and lower layers are given by σ_1 and σ_2, respectively (see Fig. 1b). The lower layer extends to infinity.

In general, θ_i depends on v and is given by

$$\theta_i^2 = v^2 + \mathrm{j}\omega\mu_0\sigma_i, \quad i = 1 \text{ or } 2. \tag{17}$$

A single-layer Earth model is easily obtained by setting $d=0$ and $\sigma_1 = 0$ in Eqs. (15)–(17). In that case, these equations can be replaced by

$$R^{1L} = \frac{(\theta - v)}{(\theta + v)}, \tag{18}$$

$$\theta^2 = v^2 + \mathrm{j}\omega\mu_0\sigma, \tag{19}$$

where σ is the conductivity of the half-space that now represents the single-layer Earth.

Eqs. (15) and (18) can be used in the integral Eqs. (12)–(14) to determine the geoelectric and geomagnetic fields at the surface of the Earth for the two- and one-layer models, respectively. The solution to the integral equations will be referred to as the exact method or exact solution.

2.3. Complex image method (CIM)

Boteler and Pirjola (1998) (hereafter referred to as BP98) present a simple derivation of the CIM expressions for the fields given by Eqs. (12)–(14). By using a complex natural exponential function to approximate R, these integral equations can be analytically solved to obtain algebraic relations for the fields at the surface of the Earth.

A complex skin depth, p, is defined as

$$p = \frac{Z}{\mathrm{j}\omega\mu_0}, \tag{20}$$

where $Z = -E_y/H_x$ is the surface impedance of the Earth. For a line current source, Z is a function of the layered conductivity structure and v (Pirjola and Viljanen, 1998). In the more general case of a 3D source, Z is a function of two horizontal wavenumbers and the layered conductivity structure (e.g., Wait, 1981, p. 192).

For a single-layer Earth model the general surface impedance for a line current source is given by

$$Z = \frac{\mathrm{j}\omega\mu_0}{\sqrt{v^2 + \mathrm{j}\omega\mu_0\sigma}}. \tag{21}$$

The reflection coefficient can then be written as

$$R = \frac{p^{-1} - v}{p^{-1} + v} = 1 - 2pv\left(\frac{1}{1 + pv}\right). \tag{22}$$

Noting the similarity of the expansion of Eq. (22) to that of a natural exponential function, BP98 approximate R with

$$R^{CIM} = \mathrm{e}^{-2pv}. \tag{23}$$

It is stated by BP98 that this approximation is exact for $(pv)^3 \ll 1$ (and we assume that $|pv|^3 \ll 1$ was the intended expression).

Finally, using Eq. (23) in the integral field expressions (12)–(14), BP98 give the CIM field equations at the surface of the Earth due to an ionospheric line current

$$B_x = \frac{\mu_0 I}{2\pi}\left(\frac{h}{h^2 + x^2} + \frac{h + 2p}{(h + 2p)^2 + x^2}\right), \tag{24}$$

$$B_z = -\frac{\mu_0 I}{2\pi}\left(\frac{x}{h^2 + x^2} + \frac{x}{(h + 2p)^2 + x^2}\right), \tag{25}$$

$$E_y = -\frac{\mathrm{j}\omega\mu_0 I}{2\pi}\ln\left[\frac{\sqrt{(h + 2p)^2 + x^2}}{\sqrt{h^2 + x^2}}\right]. \tag{26}$$

It should be noted that these equations can only be obtained if p is independent of v, that is $v = 0$ in Eq. (21). This assumption is more clearly stated by Pirjola and Boteler (2002) and corresponds to using the plane wave surface impedance for Z in Eq. (20).

The physical interpretation of the CIM equations is that the induction properties of a layered, conducting Earth can be represented by an image current, flowing in the opposite direction to the source current, at a complex depth of $h+2p$. A general formulation of the CIM is given by Thomson and Weaver (1975). The CIM equations have been extended to include distributed horizontal currents (Boteler et al., 2000) and finite-length line currents (Pirjola and Viljanen, 1998), and have been used in several studies of geomagnetic induction and GICs (Boteler, 1998; Viljanen et al., 1999a, b; Pulkkinen et al., 2000; Pirjola et al., 2000; Pirjola, 2000).

3. Comparison and discussion

The reflection coefficients described in Sections 2.2 and 2.3 are first examined for single- and two-layer Earth models. Comparisons are then made of the fields calculated using these coefficients in the integral Eqs. (12)–(14) to those obtained from the MAS.

3.1. Single-layer earth model

In the high-frequency limit ($\omega \to \infty$ and σ, v finite) $R^{1L} \to 1$ and $R^{CIM} \to 1$. That is, for high frequencies both reflection coefficients converge to the expected value of unity. In this limit, the incident fields do not penetrate the Earth and total reflection of the incident fields occurs.

At low frequencies ($\omega \to 0$ and σ, v finite) both reflection coefficients also converge to the expected value, $R^{1L} = R^{CIM} \to 0$. Zero reflection, in this case, implies that the incident fields simply penetrate the Earth and the resulting fields are due to the ionospheric current source only.

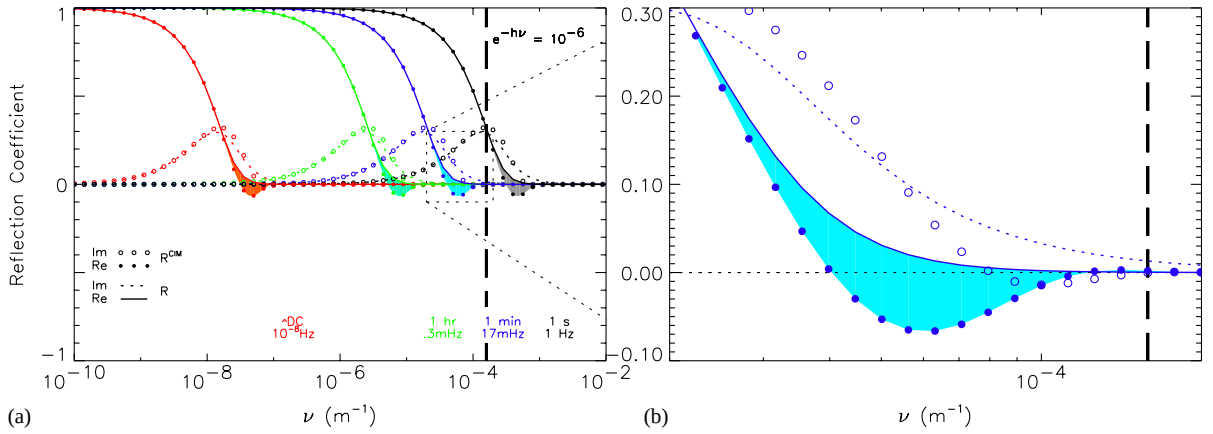

Fig. 3. (a) Reflection coefficients for a single-layer Earth model as a function of ν for four different frequencies: 1 Hz, 17 mHz, 0.3 mHz, 10^{-8} Hz. Real and imaginary components are shown for the exact solution (R) and the CIM (R^{CIM}). (b) An expanded view of (a) for 17 mHz (1 min period). A vertical dashed line near $\nu = 10^{-4}$ indicates where $e^{-h\nu}$ falls below 10^{-6} in integral Eqs., (12)–(14). Differences between the real parts of the CIM and the exact solution are indicated by shading.

While the reflection coefficient for the CIM agrees with the exact solution at high and low frequencies, there is a range of frequencies between these limits where they differ. The reason is that the form of the CIM reflection coefficient is a complex natural exponential, which decays but also oscillates. In some middle range of frequencies R^{CIM} can, therefore, be negative, suggesting a non-physical result for a diffusive situation, such as geomagnetic induction.

Fig. 3 shows the reflection coefficients as a function of ν for a single-layer Earth model with a uniform conductivity of 10^{-2} S m^{-1}. The integration limits of Eqs. (12)–(14) are strictly from 0 to ∞, but only the range $\nu = 10^{-10}$–10^{-2} m^{-1} is shown. The presence of the term $e^{-h\nu}$ makes it computationally practical to stop the integration at a finite value, which depends on the altitude of the line current. An altitude of 100 km ($h = 10^5$ m) is assumed throughout this work. For reference, a vertical dashed line is shown in Fig. 3 at the location where $e^{-h\nu} = 10^{-6}$. Values of ν higher than this reference contribute little to the solution. The real and imaginary parts are shown in Fig. 3 for four frequencies in the range of interest for geomagnetic induction: $f = 1$ Hz, ~17 mHz, ~0.3 mHz, and 10^{-8} Hz, which correspond to periods of 1 s, 1 min, 1 h, and 10^8 s, respectively (the latter being approximately DC).

It is worth noting that while the CIM and exact method curves are quite similar in Fig. 3, they are not identical. Both curves begin at the value of 1 for $\nu \to 0$ and approach 0 for larger values of ν, but they differ at intermediate values. These differences are highlighted in Fig. 3 with solid shading. An expanded view of the ~17 mHz (1 min period) curve is also shown in Fig. 3b for clarity.

The departure of the CIM curve from the exact solution can be attributed to the oscillatory component in the complex natural exponential function, $e^{-2p\nu}$. The consequence is that R^{CIM} is negative for some values of ν, and, therefore, exhibits some non-diffusive behavior. While the effect of this behavior can be small, and integration of the oscillatory portion tends to average to zero, this is not always the case, especially for more complicated multi-layer Earth models.

The geoelectric and geomagnetic fields calculated with the reflection coefficients for the single-layer Earth model, and those using the MAS are shown in Fig. 4. The frequency range (10^{-8}–1 Hz) corresponds roughly to the range of interest for geomagnetic induction. The amplitude of the line current is taken to be 1 MA, a typical value used in other studies (e.g., Boteler and Pirjola, 1998; Pirjola and Boteler, 2002). Fig. 4a, c, and e, show the B_x, B_z, and E_y field components, respectively, while Fig. 4b, d, and f show these components over a limited range of frequencies. The magnetic fields are given in nanoTeslas (nT) (a common unit used by magnetometers) and the electric field in mV m^{-1}. The curves shown are for a location on the Earth's surface ($z = 0$) km at a distance of $x = 100$ km.

The first important point to make regarding Fig. 4 is that, to within the desired numerical accuracy, the curves corresponding to the MAS solutions and the exact solutions are identical. Over the entire frequency range of interest (0–1 Hz), the MAS, therefore, reproduces the exact solution for the single-layer Earth model. Although only a single location is shown, it has been verified that the MAS matches the exact solution at all surface locations.

Also evident in Fig. 4 is that all the curves converge to the expected values for low ($< \sim 10^{-5}$ Hz) and high ($> \sim 10^{-2}$ Hz) frequencies. However, in the range $10^{-5} < f < 10^{-2}$ Hz the CIM and the exact solution differ. This frequency range corresponds roughly to periods of 1 min to 1 day. The differences in the B_x and B_z components are as high as 40 nT for some frequencies, while the

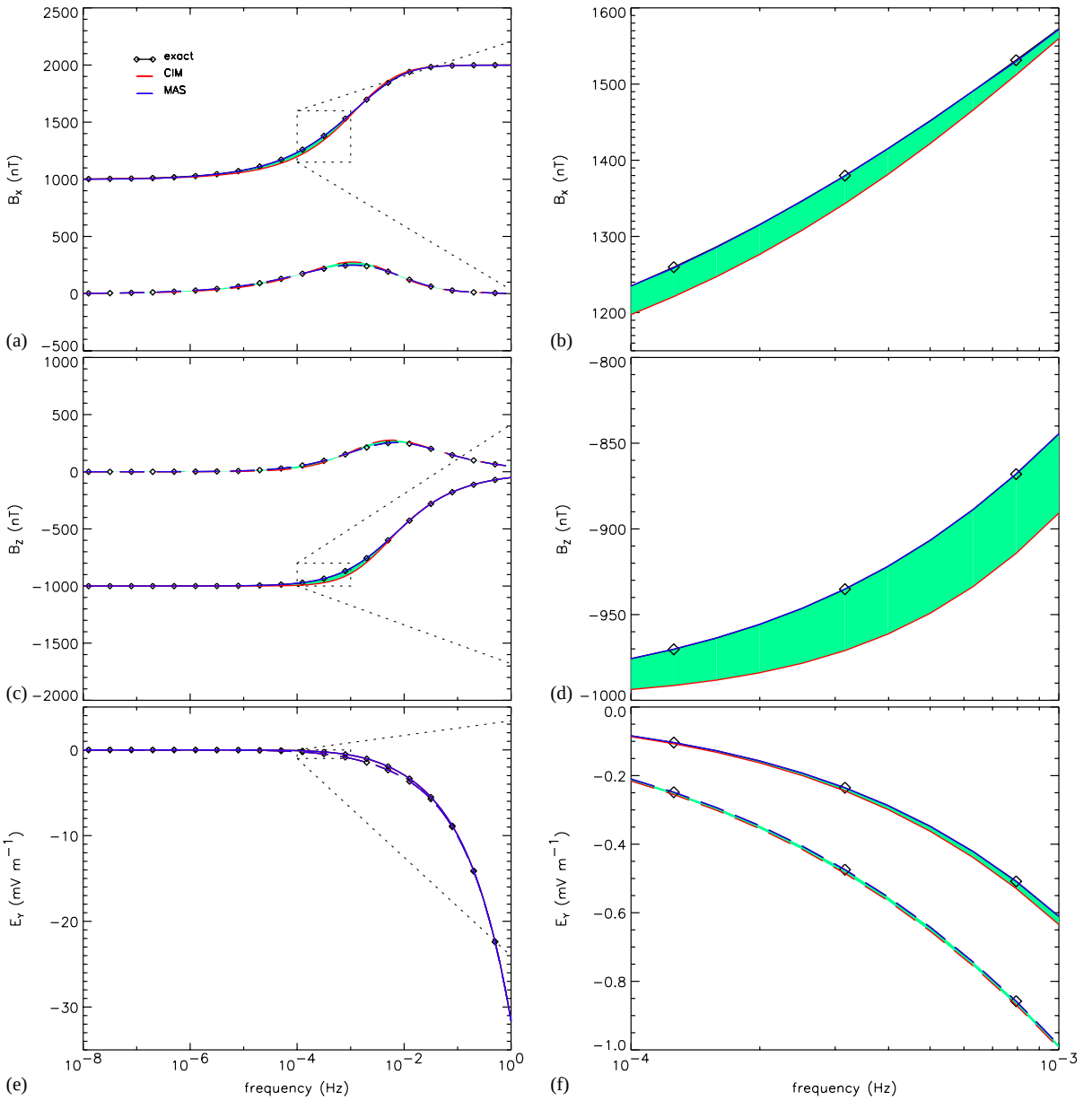

Fig. 4. Electric (E_y) and magnetic fields (B_x and B_z) at the surface ($z = 0$, $x = 100$ km) of a 1D Earth model with uniform conductivity $\sigma = 10^{-2}$ S m^{-1}. The fields are calculated using the MAS, the CIM, and the exact solution for a 1 MA ionospheric line current located at ($z = -h$, $x = 0$).

difference in E_y, for this particular example, is relatively small, at most only $\sim$0.025 mV m^{-1}.

It is easy to see from Fig. 3 why these differences appear in the range $\sim 10^{-5}$–10^{-2} Hz. For these frequencies there are values of v for which R^{CIM} is both negative and the term e^{-hv} is not yet sufficiently small that the contribution to the integrals in Eqs. (12)–(14) is negligible. Differences in the fields arise only if the small range of v, for which R^{CIM} differs from the exact value, falls near but below the e^{-hv} 'cutoff'. For frequencies above $\sim 10^{-2}$ Hz, the two reflection coefficients are identical over the range of v below the cutoff (see 1 s period curve in Fig. 3). For the frequencies below $\sim 10^{-5}$ Hz, the differences occur over a negligible range of v. The frequency range for which R^{CIM} differs from the exact solution depends on both σ and h.

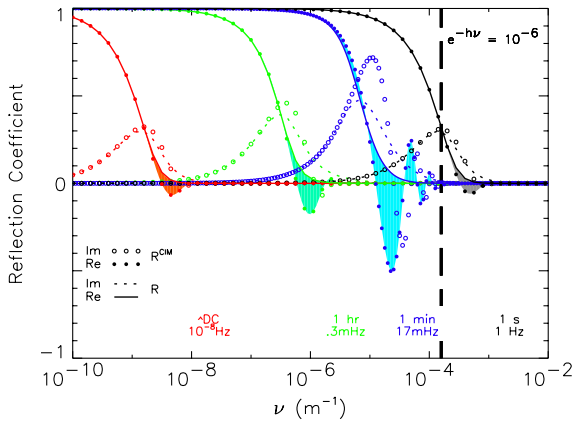

Fig. 5. Reflection coefficients for a two-layer Earth model consisting of a top layer (d=10 km) and a lower semi-infinite half-space layer. Conductivities for the upper and lower layers are $\sigma_1 = 10^{-2}$ S m^{-1} and $\sigma_2 = 10^{-4}$ S m^{-1}, respectively.

3.2. Two-layer earth model

Fig. 5 shows R and R^{CIM} for the slightly more complicated two-layer Earth model (shown in Fig. 1b) in the same format as Fig. 3. For this example the thickness of the first layer is chosen to be d=10 km, and the conductivities of the top and bottom layers as $\sigma_1 = 10^{-2}$ S m^{-1} and $\sigma_2 = 10^{-4}$ S m^{-1}, respectively.

For this case, the amplitude of the oscillations of R^{CIM} become quite significant in a band of frequencies near 17 mHz and the departure from the exact solution is correspondingly large. It is, therefore, expected that significant differences exist in the fields obtained from the CIM and the exact method for frequencies near ~17 mHz.

Fig. 6 shows the fields obtained from the different methods for the two-layer Earth model. The frequency range (10^{-4}–10^{-1} Hz) is chosen to highlight only the differences in the methods. Again, the MAS curves are indistinguishable from the exact solution over the entire frequency range confirming the accuracy of this technique. On the other hand, as suggested from the reflection coefficients, the CIM and the exact solution differ considerably in this case. The CIM can be in error by as much as 300 nT in the magnetic field and as much as 2 mV m^{-1} in the electric field.

It is emphasized that the model of the Earth conductivity used in this example is not intended to represent any particular geological feature but rather to demonstrate the accuracy of the MAS. There are, however, many examples in the literature of both two-layer Earth models with parameters similar to those of our example (e.g., Peltier and Hermance, 1971), and more complicated multi-layer models (e.g., Boteler and Pirjola, 1998; Pirjola and Boteler, 2002). In a two-layer model the magnitude of the observed differences and the frequency range over which they manifest are determined by the thickness of the top layer, the height of the ionospheric line current, and the relative conductivities of the layers. It is, therefore, possible that for more complicated multi-layer models several frequency bands exist for which non-negligible errors occur when using the CIM. For situations in which accuracy is of concern, the MAS is a suitable alternative.

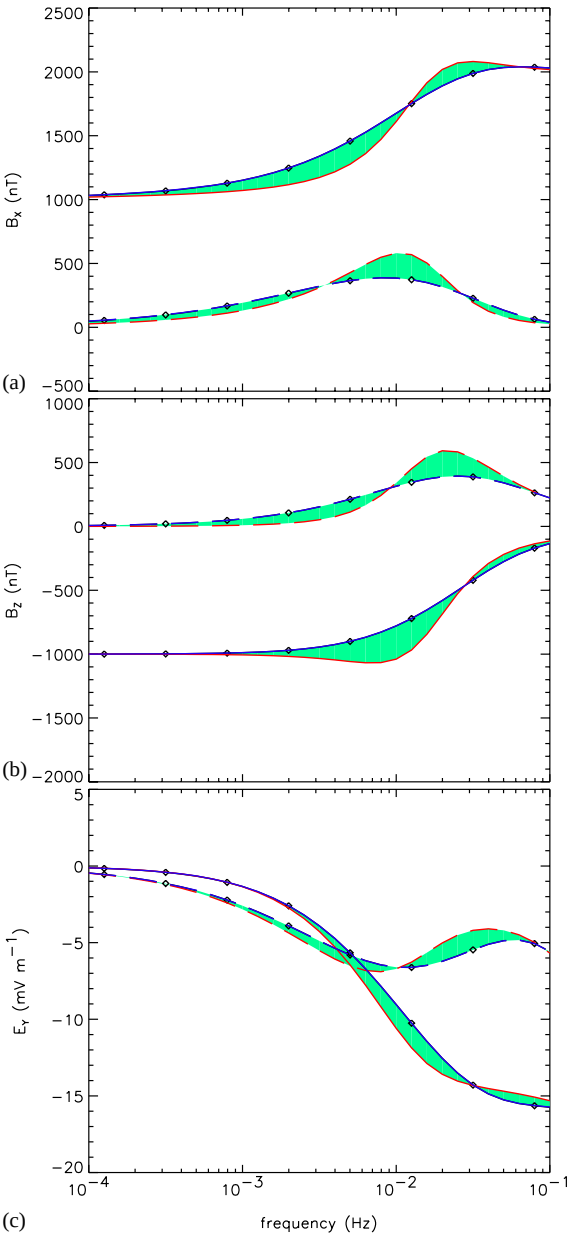

Fig. 6. Electric (E_y) and magnetic fields (B_x and B_z) as described in Fig. 4 but for a 1D, two-layer Earth model with upper and lower layer conductivities of $\sigma_1 = 10^{-2}$ S m^{-1} and $\sigma_2 = 10^{-4}$ S m^{-1}, respectively.

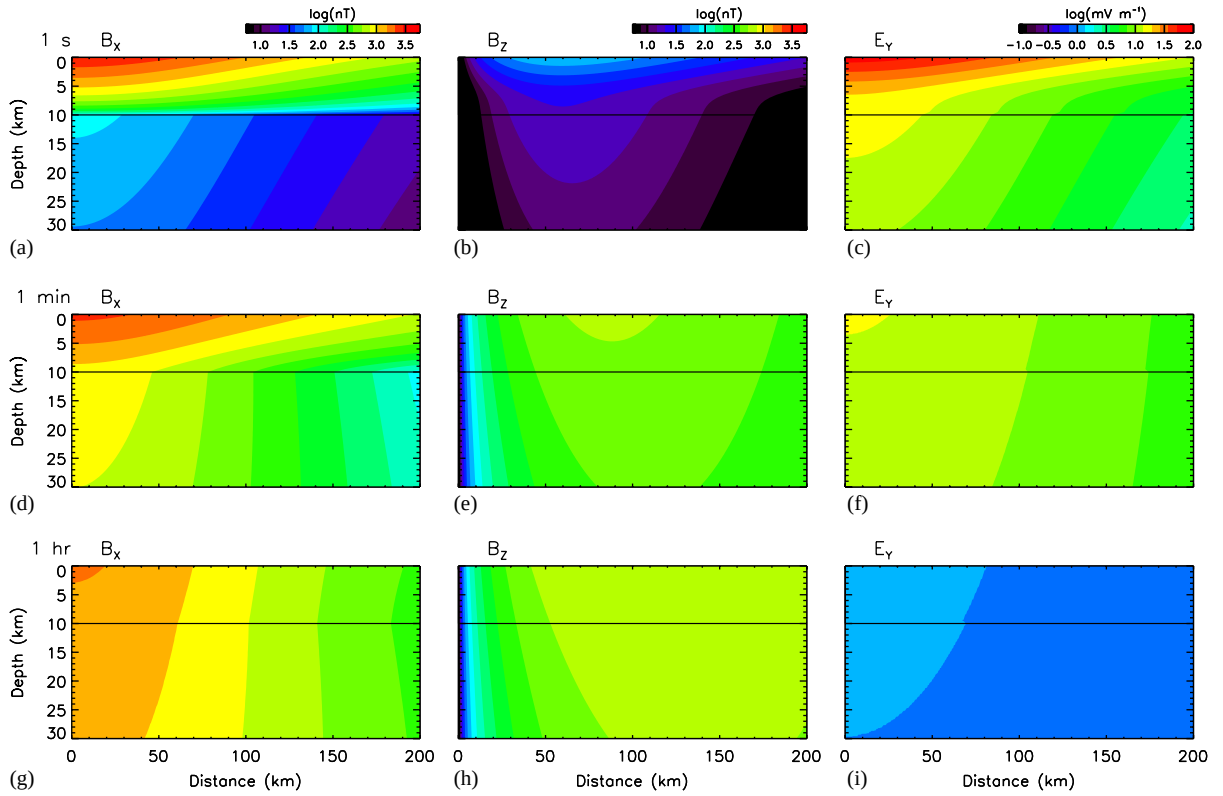

Fig. 7. Geoelectric and geomagnetic fields inside the two-layer Earth model shown in Fig. 1b. Contours correspond to the magnitude of fields due to a 1 MA line current located at $z = -100$ km and $x = 0$ km. Three periods are shown: (a–c) 1 s, (d–f) 1 min, and (g–i) 1 h.

3.3. Fields inside earth

The two simple examples in Sections 3.1 and 3.2 serve to illustrate the accuracy of the MAS in calculating the geoelectric and geomagnetic fields at the surface of the Earth. The MAS, as described in Section 2.1, however, is not limited to specifying the fields at the surface. Once the amplitudes of the auxiliary line currents are determined the vector potentials given by Eqs. (8) and (11) are physically meaningful in both regions 1 and 2, and the electric and magnetic fields can be computed rapidly at any desired spatial resolution in these regions.

Fig. 7 shows the magnitude of the fields 'inside' the Earth for the two-layer Earth model. The extent of the domain shown corresponds to the quasi-near field due to the line current source located at $x = 0$ km and $z = -100$ km. The fields are calculated using the MAS for periods of 1 s (Fig. 7a–c), 1 min (Fig. 7d–f), and 1 h (Fig. 7g–i). The color bar above each column indicates the magnitude of the field shown by contours in the panels below (phase information has been suppressed.) Note that the scales for the B_x and B_z components are the same.

The overall expected behavior of the fields in this case is evident from Fig. 7. The magnitude of the fields fall off with depth and increase with frequency, the B_x and E_y components are maximum directly underneath the source current, while the B_z component is zero, and the B_z component maximizes (for a given depth) at a distance that depends on the height of the current source and the frequency. As expected, the fields penetrate further at lower frequencies. The penetration distance or skin depth, δ, for plane waves is proportional to $1/\sqrt{\omega\sigma}$. For the 1 s case, the bottom layer is shielded quite effectively by currents flowing in the top layer and the magnetic field is nearly horizontal. As the frequency decreases, all of the field components penetrate further and eventually become nearly uniform with depth for the 1 h case.

The dependence of δ on conductivity can also be seen in Fig. 7. Because the lower layer is 100 times less conducting than the top layer, the fields penetrate more effectively in the bottom layer. Fig. 7a–c show this behavior particularly well. In these figures the fields are continuous across the conductivity interface at $z = -10$ km, but the fields are more uniform with depth in the lower layer than in the upper. At low frequencies the differences in conductivity become less important and the field penetrates into both layers effectively.

It is possible using the MAS to plot curves similar to Figs. 4 and 6, or the fields versus position for a fixed frequency, at any 2D position. These curves may be useful in situations for which the fields below the Earth's surface are

of importance. It is certainly the case that the ability to calculate 2D fields will be useful in investigating geomagnetic induction in more complicated situations.

4. Conclusions

It has been shown that the MAS, originally developed for a wide class of scattering and excitation problems, is accurate for large-scale (>1 km), low-frequency (0–1 Hz) geomagnetic induction problems. In particular, a 2D frequency domain code was developed to compare the magnetic and electric fields induced at the surface of layered Earth models by an ionospheric line current, to those given by the CIM and the exact solution. The fields calculated using the MAS are indistinguishable from those obtained using the exact integral solution to Maxwell's equations over the entire frequency range. In addition to accuracy, the MAS is not limited to 1D models of the Earth's conductivity. It is this aspect of the MAS, perhaps more than any other, that suggests the possibilities of this technique in studying geomagnetic induction problems. At the very least, the MAS is another technique for use in accurately calculating the geoelectric and geomagnetic fields in the Earth. The combined accuracy and flexibility of this technique suggests, however, that a new level of understanding may be achieved through applying the MAS to complicated geomagnetic induction problems.

Acknowledgements

We thank William Lotko and David H. Boteler for valuable discussions about electromagnetics, geomagnetic induction, and the CIM. We also thank Ari Viljanen for assistance with the CIM code. This work was supported by NOAA Grant NA06RP0509 and the NASA Sun-Earth Connection Theory Program Grant NAG5-11735.

References

Anastassiu, H.T., Kaklamani, D.I., Economou, D.P., Breinbjerg, O., 2002. Electromagnetic scattering analysis of coated conductors with edges using the method of auxiliary sources in conjunction with the standard impedance boundary condition (sibc). IEEE Transactions on Antennas and Propagation 50, 59.

Boteler, D.H., 1998. Geomagnetic effects on electrical systems. Physics in Canada 54, 332.

Boteler, D.H., Pirjola, R.J., 1998. The complex-image method for calculating the magnetic and electric fields produced at the surface of the Earth by the auroral electrojet. Geophysical Journal International 132, 31.

Boteler, D.H., van Beek, G.J., 1999. August 4, 1972 revisited: a new look at the geomagnetic disturbance that caused the L4 cable system outage. Geophysical Research Letters 26, 577.

Boteler, D.H., Pirjola, R.J., Nevanlinna, H., 1998. The effects of geomagnetic disturbances on electrical systems at the earth's surface. Advances in Space Research 22, 17.

Boteler, D.H., Pirjola, R., Trichtchenko, L., 2000. On calculating the electric and magnetic fields produced in technological systems at the Earth's surface by a "wide" electrojet. Journal of Atmospheric and Solar-Terrestrial Physics 62, 1311.

Hermance, J.F., Peltier, W.R., 1970. Magnetotelluric fields of a line current. Journal of Geophysical Research 75, 3351.

Kaufman, A.A., Keller, G.V., 1981. The Magnetotelluric Sounding Method. Elsevier Scientific Publishing Company, Amsterdam.

Lehtinen, M., Pirjola, R., 1985. Currents produced in earthed conductor networks by geomagnetically-induced electric fields. Annales de Geophysique 3, 479.

Molinski, T.S., Feero, W.S., Damsky, B.L., 2000. Shielding grids from solar storms. IEEE Spectrum, 37, 55.

Peltier, W.R., Hermance, J.F., 1971. Magnetotelluric fields of a gaussian electrojet. Canadian Journal of Earth Sciences 8, 338.

Pirjola, R., 2000. Geomagnetically induced currents during magnetic storms. IEEE Transactions on Power Systems 28, 1867.

Pirjola, R., Boteler, D., 2002. Calculation methods of the electric and magnetic fields at the Earth's surface produced by a line current. Radio Science 37, 10.1029/2001RS002576.

Pirjola, R., Viljanen, A., 1998. Complex image method for calculating electric and magnetic fields produced by an auroral electrojet of finite length. Annales de Geophysique 16, 1434.

Pirjola, R., Boteler, D., Viljanen, A., Amm, O., 2000. Predictions of geomagnetically induced currents in power transmission systems. Advances in Space Research 26, 5.

Pulkkinen, A., Viljanen, A., Pirjola, R., BEAR Working Group, 2000. Large geomagnetically induced currents in the Finnish high-voltage power system. Technical Report 2, Finnish Meteorological Institute.

Shubitidze, F., O'Neill, K., Paulsen, K., 2001. The method of auxiliary sources for analysis low frequency EM field scattering from composite objects. 2001 IEEE Antennas and Propagation Society International Symposium, July 8–13, Boston, MA.

Shubitidze, F., Anastassiu, H., Kaklamani, D., 2002a. An improved accuracy version of the method of auxiliary sources for computational electromagnetics. IEEE Transactions on Antennas and Propagation, in press.

Shubitidze, F., O'Neill, K., Haider, S.A., Sun, K., Paulsen, K.D., 2002b. Application of the method of auxiliary sources to the wideband electromagnetic induction problem. IEEE Transactions on Geoscience and Remote Sensing 40, 928.

Shubitidze, F., O'Neill, K., Shamatava, I., Sun, K., Paulsen, K., 2002c. Implementation of hybrid MAS and SPA algorithm for broadband electromagnetic induction problems. VII-International Workshop on Direct and Inverse Problems of Electromagnetic and Acoustic Wave Theory (DIPED-2002), Tbilisi, Georgia, October 10–13.

Shubitidze, F., O'Neill, K., Sun, K., Paulsen, K.D., 2002d. Investigation of broadband electromagnetic induction scattering by highly conducting, permeable, arbitrarily shaped 3D objects. IEEE Transactions on Geoscience and Remote Sensing, in press.

Thomson, D.J., Weaver, J.T., 1975. The complex image approximation for induction in a multilayered earth. Journal of Geophysical Research 80, 123.

Viljanen, A., Amm, O., Pirjola, R., 1999a. Modeling geomagnetically induced currents during different ionospheric situations. Journal of Geophysical Research 104, 28,059.

Viljanen, A., Pirjola, R., Amm, O., 1999b. Magnetotelluric source effect due to 3D ionospheric current systems using the complex image method for 1D conductivity structures. Earth Planets and Space 51, 933.

Wait, J.R., 1981. Geo-Electromagnetism. Academic Press, New York.